Parton branching model for $p\bar{p}$ collisions

A. H. Chan and C. K. Chew
Department of Physics, National University of Singapore, Kent Ridge, 0511 Singapore
(Received 8 May 1989)

A detailed analysis of the behavior of the initial numbers of gluons and quarks in the generalized multiplicity distribution (GMD) is presented. Two special cases of GMD, namely, the negative-binomial distribution and the Furry-Yule distribution, are also discussed in relation to the non-single-diffractive data at 200, 546, and 900 GeV c.m.-system energies and pseudorapidity intervals η_c. The GMD may provide an alternate distribution to understand parton action for future $p\bar{p}$ collisions at high TeV energies.

I. INTRODUCTION

Recently, it was reported by UA5 (Ref. 1) that the well-known negative-binomial distribution (NBD) fails to fit 900-GeV non-single-diffractive (NSD) data for large pseudorapidity intervals in the peak region of the distribution. UA5 further examined other models, namely, the partially coherent laser distribution (PCLD), which is supported by quantum-statistical arguments, and the dual parton models PYTHIA and FRITIOF models (DPM's) which assume that hadrons are produced via chains or strings. However, just as for the NBD, the χ^2 fits are generally much too large to describe the 900-GeV data satisfactory for large intervals and the full phase space.

Our main thrust of this paper is to examine the generalized parton branching model based on the generalized multiplicity distribution (GMD) (Ref. 2).

From QCD, let t be the natural evolution parameter, where

$$t=\frac{6}{11N_c-2N_f}\ln\left[\frac{\ln(Q^2/\mu^2)}{\ln(Q_0^2/\mu^2)}\right] \tag{1}$$

and Q is the initial parton invariant mass, Q_0 is the hadronization mass, μ is a few GeV (a QCD mass scale), $N_c=3$ (number of colors), and $N_f=4$ (number of flavors). Given certain initial conditions we can write down the probability for producing n gluons and m quarks, through the following Markov branching processes:

(i) A: $g\rightarrow g+g$,

(ii) $\tilde{A}$: $q\rightarrow q+g$,

(iii) B: $q\rightarrow q+\bar{q}$,

(iv) C: $g\rightarrow g+g+g$

in the interval $t+\Delta t$ within the constraint of the conservation of total probability. Hence,

$$\begin{aligned}P_{m,n}(t+\Delta t)=&(1-An\,\Delta t-\tilde{A}m\,\Delta t-Bn\,\Delta t-Cn\,\Delta t)P_{m,n}(t)+A(n-1)\Delta t\,P_{m,n-1}(t)+\tilde{A}m\,\Delta t\,P_{m,n-1}(t)\\&+B(n+1)\Delta t\,P_{m-2,n+1}(t)+C(n-2)\Delta t\,P_{m,n-2}(t)\ .\end{aligned} \tag{2}$$

For the first approximation

$$P_{m,n}(t+\Delta t)=P_{m,n}(t)+\frac{\partial P_{m,n}(t)}{\partial t}\Delta t\ . \tag{3}$$

TABLE I. Comparison of χ^2/points for GMD, NBD, and FYD at 200 GeV (limited pseudorapidity ranges) and within parentheses the numbers of data points being taken.

		GMD			NBD		FYD	
η_c	$\langle n\rangle$	k'	k	χ^2/points	k	χ^2/points	k'	χ^2/points
0.5	2.50	0.01	1.83	0.94 (12)	1.86	0.90 (12)	0.88	48.51 (12)
							0.81	6.13 (11)
1.5	7.94	0.01	2.22	0.63 (36)	2.23	0.63 (36)	1.00	10.46 (36)
							1.60	2.80 (35)
3.0	15.50	0.80	1.93	0.26 (50)	3.06	0.29 (50)	1.00	20.35 (50)
							2.00	0.64 (49)
5.0	20.50	0.80	2.88	0.22 (55)	3.99	0.22 (55)	1.00	14.37 (55)
							2.00	2.88 (54)

TABLE II. Comparison of χ^2/points for GMD, NBD, and FYD at 546 GeV (limited pseudorapidity ranges) and within parentheses the number of data points being taken.

		GMD			NBD		FYD	
η_c	$\langle n \rangle$	k'	k	χ^2/points	k	χ^2/points	k'	χ^2/points
0.5	3.01	0.01	1.76	1.23 (21)	1.79	1.20 (21)	1.00	52.84 (21)
							0.89	9.10 (20)
1.5	9.49	0.01	2.16	1.28 (26)	1.94	0.94 (26)	1.00	58.62 (26)
							1.52	4.43 (25)
3.0	18.90	0.30	2.08	1.11 (29)	2.47	1.14 (29)	1.00	179.50 (29)
							2.04	1.84 (28)
5.0	26.40	0.01	3.08	0.96 (33)	3.09	0.96 (33)	1.00	511.88 (33)
							2.50	1.84 (32)

One can write the Markov branching evolution equation as

$$\frac{\partial P_{m,n}(t)}{\partial t} = -AnP_{m,n}(t) - BnP_{m,n}(t) - \tilde{A}mP_{m,n}(t) - CnP_{m,n}(t) + A(n-1)P_{m,n-1}(t) + \tilde{A}mP_{m,n-1}(t) + B(n+1)P_{m-2,n+1}(t) + C(n-2)P_{m,n-2}(t) \; . \tag{4}$$

Equation (4) was also obtained by Durand and Sarcevic,[3] however Chew, Kiang, and Zhou[2] neglected the branchings $g \rightarrow q + \bar{q}$ and $g \rightarrow g + g + g$ where $B = C = 0$.

Now the differential equation (4) becomes

$$\frac{\partial P_{m,n}(t)}{\partial t} = -\tilde{A}mP_{m,n}(t) + \tilde{A}mP_{m,n-1}(t) - AnP_{m,n}(t) + A(n-1)P_{m,n-1}(t) \; . \tag{5}$$

Solving Eq. (5) analytically, one arrives at the following general solution:

$$P_{m,n}(t) = \frac{\Gamma(n+k)}{\Gamma(n-k'+1)\Gamma(k'+k)} \times e^{-(k'+k)At}(1-e^{-At})^{n-k'} \; , \tag{6}$$

interpreting $k = m\tilde{A}/A$ where m and k' are the initial number of quarks and gluons, respectively.

Introducing the mean gluon multiplicity, $\bar{n}$ as a function of t in the intermediate stage of the branching process, we can obtain

$$\bar{n}(t) = (k'+k)e^{At} - k \tag{7}$$

from the probability generating function

$$G(x,t) = \sum_n P_{m,n}(t)x^n \; .$$

The final hadronization in the multiparticle production is given by GMD which can be expressed as

$$P_n(\bar{n},k',k) = \frac{\Gamma(n+k)}{\Gamma(n-k'+1)\Gamma(k'+k)} \times \left[\frac{\bar{n}-k'}{\bar{n}+k}\right]^{n-k'} \left[\frac{k'+k}{\bar{n}+k}\right]^{k'+k} , \tag{8}$$

TABLE III. Comparison of χ^2/points for GMD, NBD, and FYD at 900 GeV (limited pseudorapidity ranges) and within parentheses the number of data points being taken.

		GMD			NBD		FYD	
η_c	$\langle n \rangle$	k'	k	χ^2/points	k	χ^2/points	k'	χ^2/points
0.5	3.61	0.10	1.34	0.03 (20)	1.52	0.05 (20)	1.00	15.47 (20)
							0.89	3.09 (19)
1.5	11.20	0.10	1.65	0.44 (51)	1.77	0.44 (51)	1.00	5.31 (51)
							1.42	0.81 (50)
3.0	22.40	1.00	0.98	0.54 (74)	2.15	0.59 (74)	1.00	8.54 (74)
							1.86	0.50 (73)
5.0	32.50	1.00	1.73	0.62 (93)	2.97	0.72 (93)	1.00	53.71 (93)
							2.00	1.36 (92)

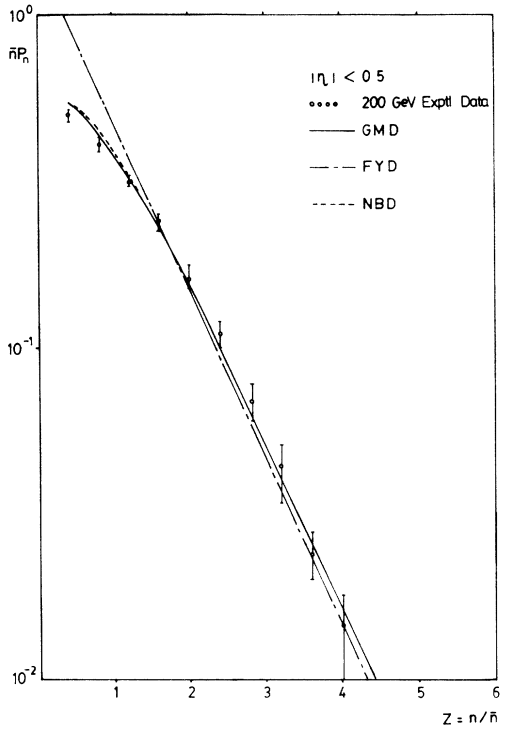

FIG. 1. Charged-multiplicity distribution (GMD, NBD, FYD) in the pseudorapidity range $|\eta| < 0.5$ at 200 GeV ($\bar{n}P_n$ vs $Z = n/\bar{n}$).

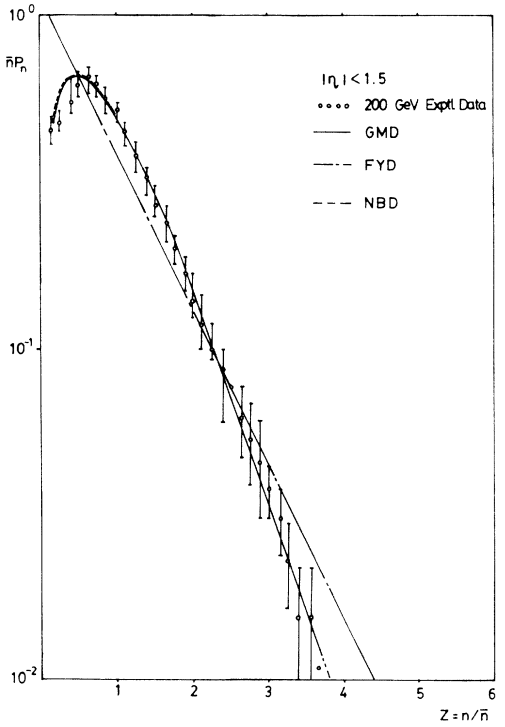

FIG. 2. Charged-multiplicity distribution (GMD, NBD, FYD) in the pseudorapidity range $|\eta| < 1.5$ at 200 GeV ($\bar{n}P_n$ vs $Z = n/\bar{n}$).

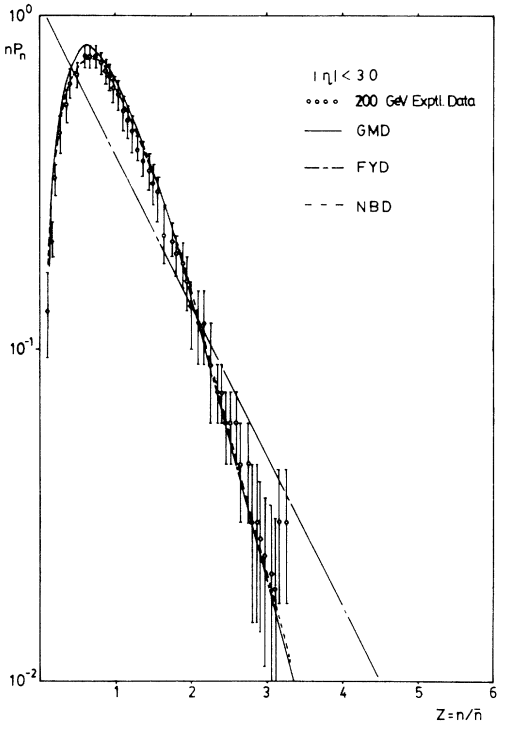

FIG. 3. Charged-multiplicity distribution (GMD, NBD, FYD) in the pseudorapidity range $|\eta| < 3.0$ at 200 GeV ($\bar{n}P_n$ vs $Z = n/\bar{n}$).

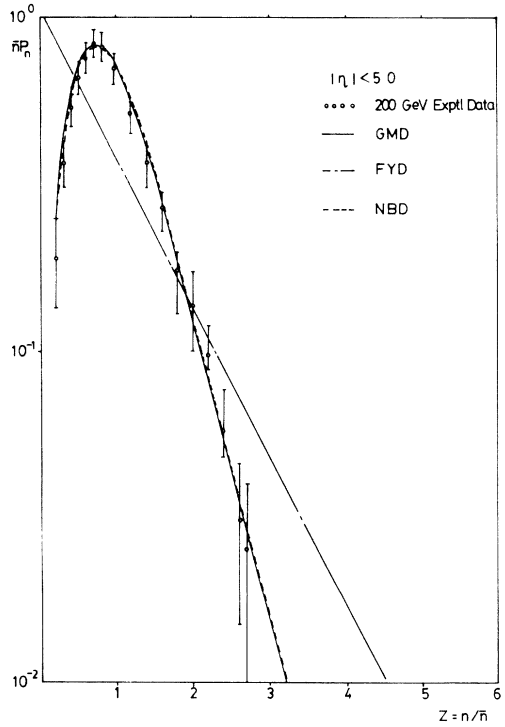

FIG. 4. Charged-multiplicity distribution (GMD, NBD, FYD) in the pseudorapidity range $|\eta| < 5.0$ at 200 GeV ($\bar{n}P_n$ vs $Z = n/\bar{n}$).

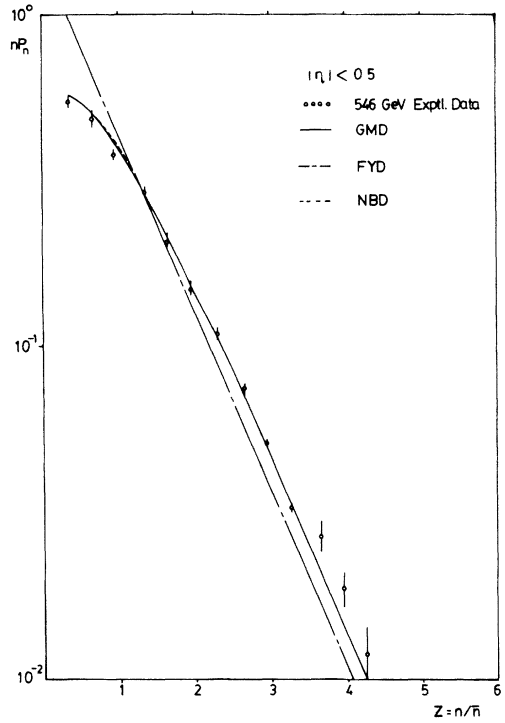

FIG. 5. Charged-multiplicity distribution (GMD, NBD, FYD) in the pseudorapidity range $|\eta| < 0.5$ at 546 GeV ($\bar{n}P_n$ vs $Z = n/\bar{n}$).

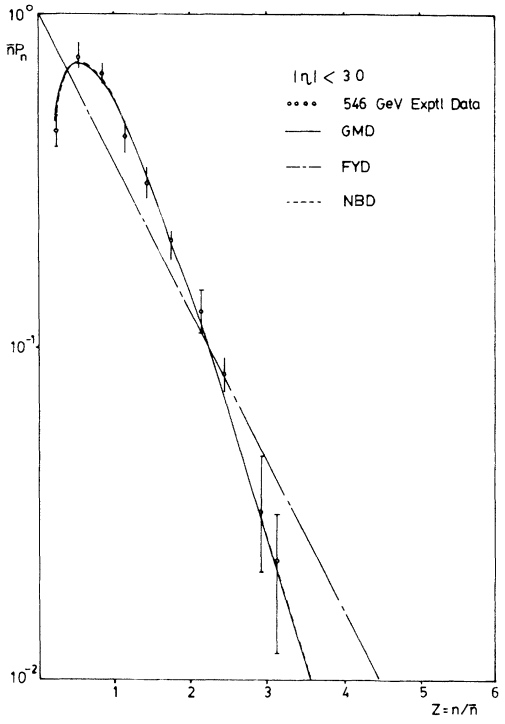

FIG. 7. Charged-multiplicity distribution (GMD, NBD, FYD) in the pseudorapidity range $|\eta| < 3.0$ at 546 GeV ($\bar{n}P_n$ vs $Z = n/\bar{n}$).

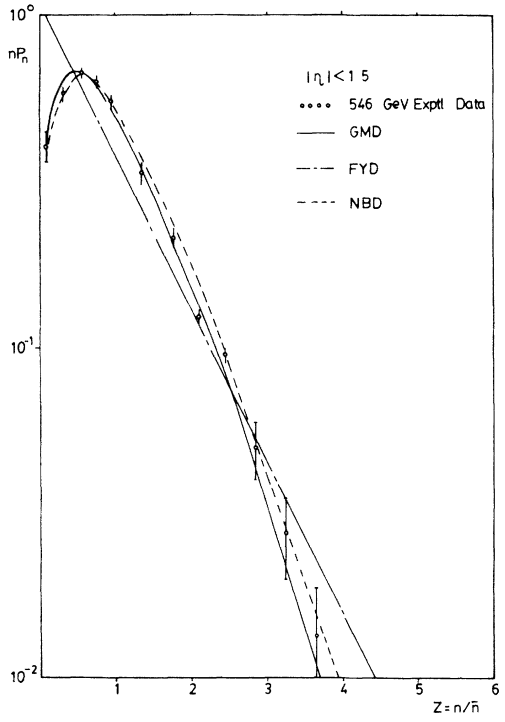

FIG. 6. Charged-multiplicity distribution (GMD, NBD, FYD) in the pseudorapidity range $|\eta| < 1.5$ at 546 GeV ($\bar{n}P_n$ vs $Z = n/\bar{n}$).

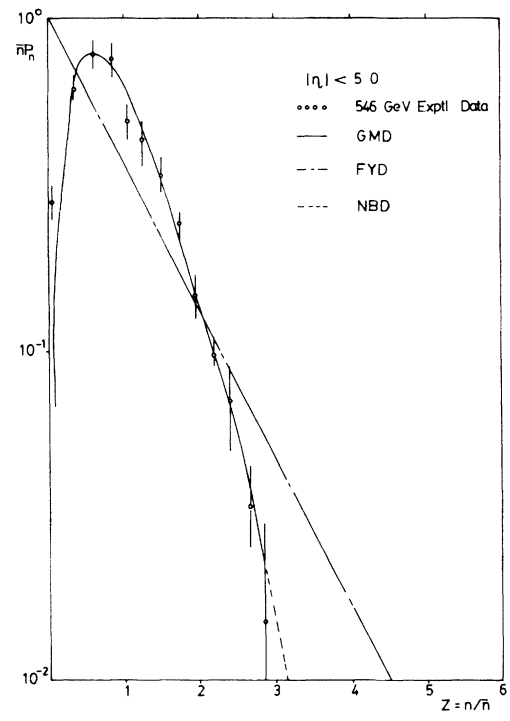

FIG. 8. Charged-multiplicity distribution (GMD, NBD, FYD) in the pseudorapidity range $|\eta| < 5.0$ at 546 GeV ($\bar{n}P_n$ vs $Z = n/\bar{n}$).

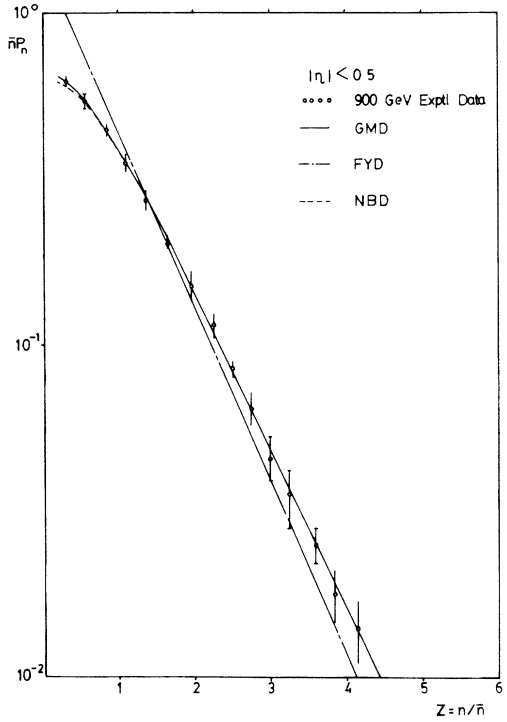

FIG. 9. Charged-multiplicity distribution (GMD, NBD, FYD) in the pseudorapidity range $|\eta|<0.5$ at 900 GeV ($\bar{n}P_n$ vs $Z=n/\bar{n}$).

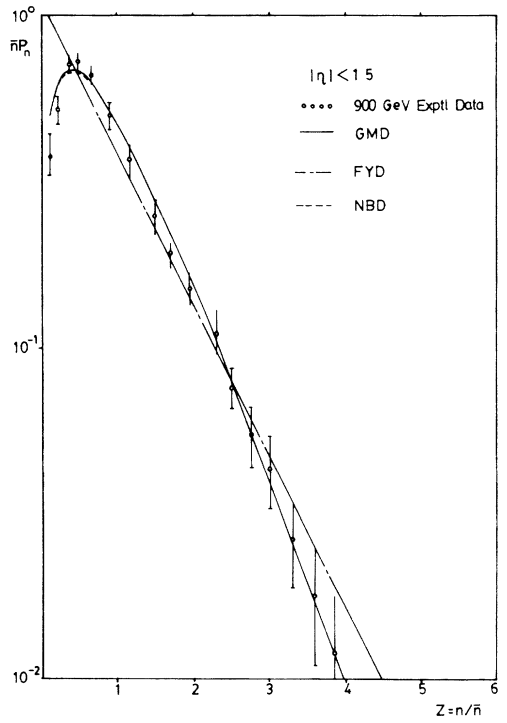

FIG. 10. Charged-multiplicity distribution (GMD, NBD, FYD) in the pseudorapidity range $|\eta|<1.5$ at 900 GeV ($\bar{n}P_n$ vs $Z=n/\bar{n}$).

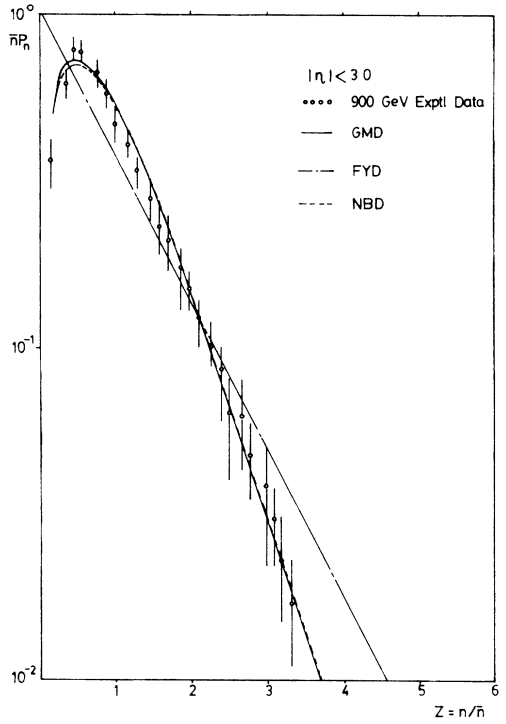

FIG. 11. Charged-multiplicity distribution (GMD, NBD, FYD) in the pseudorapidity range $|\eta|<3.0$ at 900 GeV ($\bar{n}P_n$ vs $Z=n/\bar{n}$).

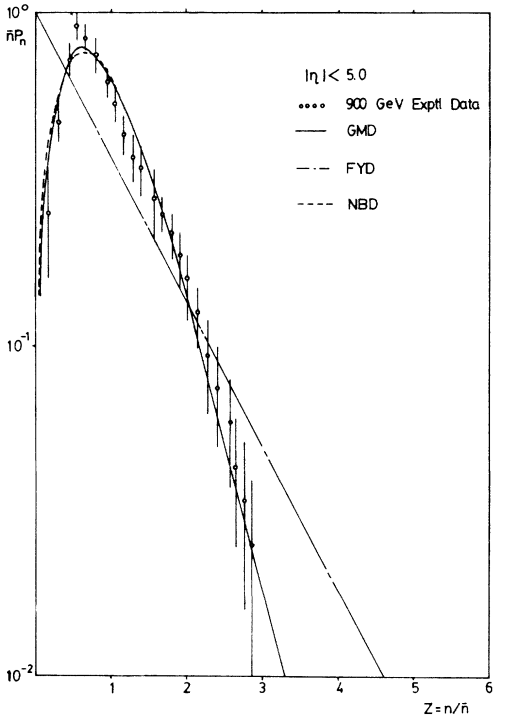

FIG. 12. Charged-multiplicity distribution (GMD, NBD, FYD) in the pseudorapidity range $|\eta|<5.0$ at 900 GeV ($\bar{n}Pn$ vs $Z=n/\bar{n}$).

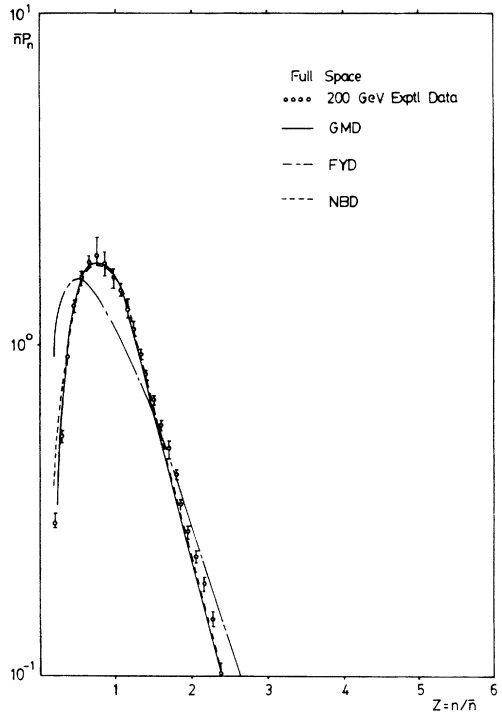

FIG. 13. Charged-multiplicity distribution (GMD, NBD, FYD) in full phase space (200 GeV).

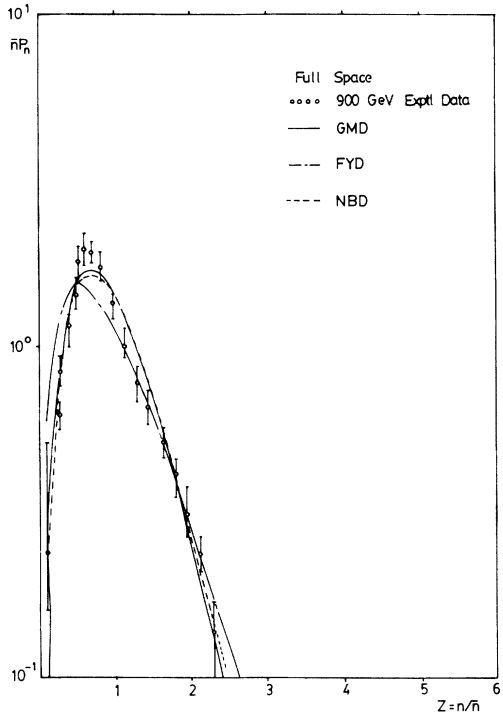

FIG. 15. Charged-multiplicity distribution (GMD, NBD, FYD) in full phase space (900 GeV).

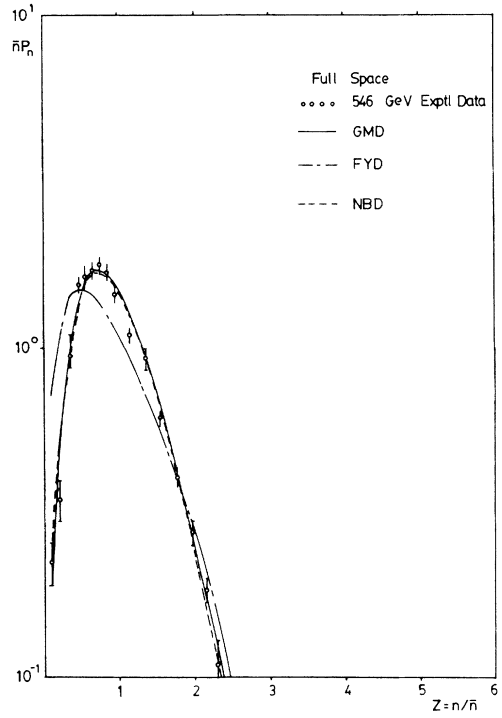

FIG. 14. Charged-multiplicity distribution (GMD, NBD, FYD) in full phase space (546 GeV).

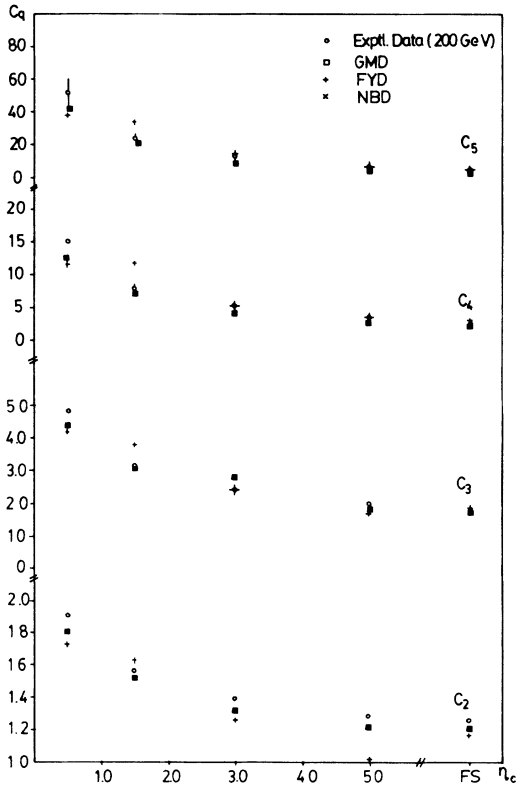

FIG. 16. C_q moments as a function of η_c at 200 GeV.

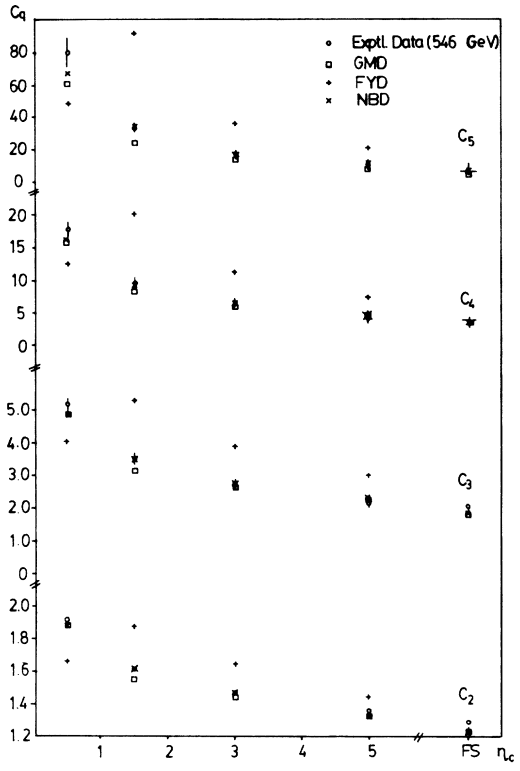

FIG. 17. C_q moments as a function of η_c at 546 GeV.

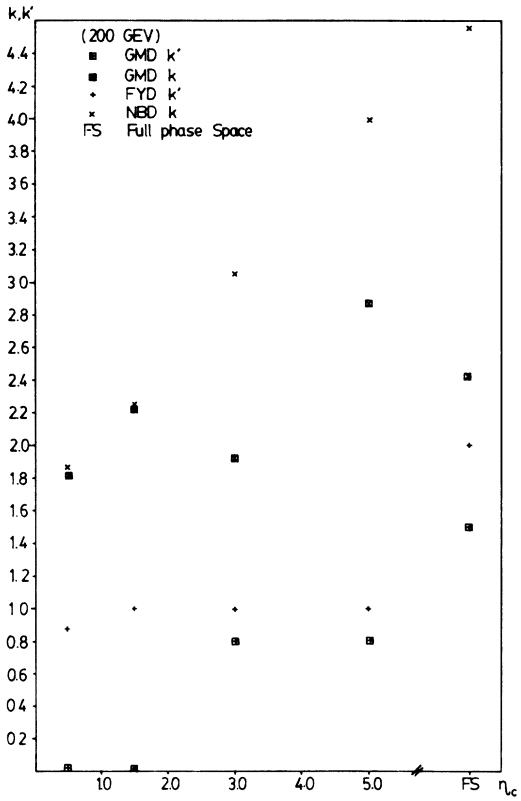

FIG. 19. k and k' plotted against η_c at 200 GeV.

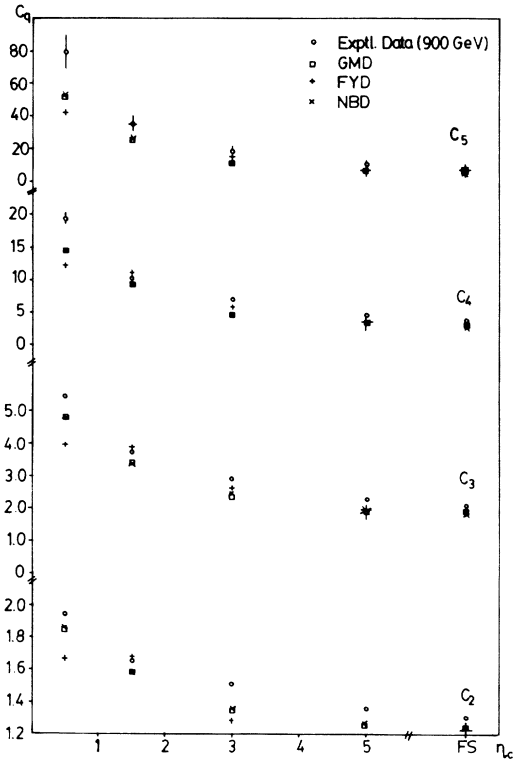

FIG. 18. C_q moments as a function of η_c at 900 GeV.

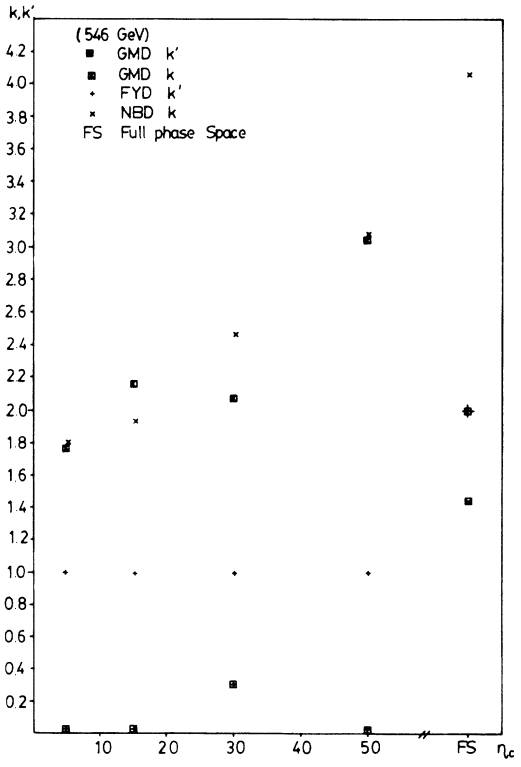

FIG. 20. k and k' plotted against η_c at 546 GeV.

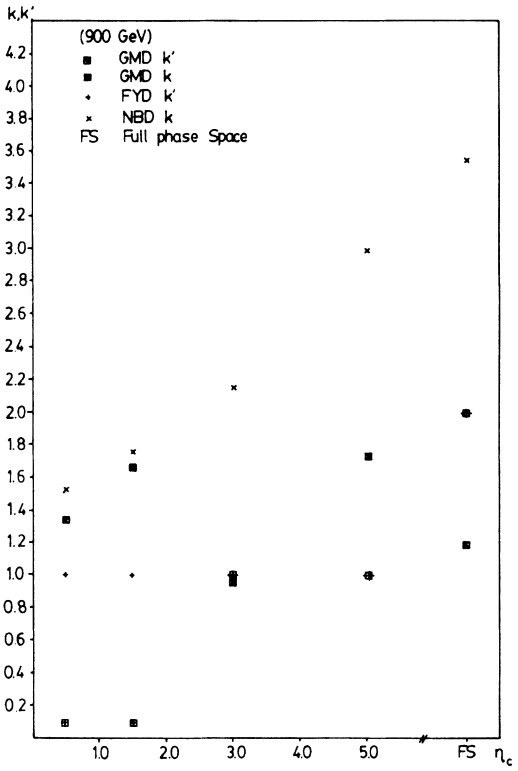

FIG. 21. k and k' plotted against η_c at 900 GeV.

where $n \geq k'$ and $\bar{n}$, the mean hadron multiplicity. The parameter $\bar{n}$ gives the average of the distribution. By fixing $\bar{n}$, the other two parameters k' and k determines the shape of the GMD.

II. SPECIAL CASES

(i) There is a similar feature in PCLD and GMD though both are clearly different in details. Both could reduce to NBD under certain conditions. Equation (8) simplifies to the following if $k'=0$:

$$P_n(\bar{n},0,k)=\frac{\Gamma(n+k)}{\Gamma(n+1)\Gamma(k)}\left[\frac{\bar{n}}{\bar{n}+k}\right]^n\left[\frac{k}{\bar{n}+k}\right]^k, \tag{9}$$

where k takes an integer values, Eq. (9) is known as the generalized Bose-Einstein distribution (GBED) and in particular when $k=1$, it is known as the geometric distribution (simple GBED). When the limit $k\to\infty$, Eq. (9) becomes the Poisson distribution and $\bar{n}\to\infty$, NBD tends to a gamma distribution. Of course, if k is a $+ve$ we have the ordinary negative-binomial distribution.

From Eq. (7), the mean gluon multiplicity is $\bar{n}(t)=k(e^{At}-1)$, a case where initially there are m quarks and no gluons, $k'=0$. The shape of the GMD and NBD can be quantified by the normalized moments

$$C_q=\frac{\overline{n^q}}{\bar{n}^q}. \tag{10}$$

Moments $q=2-5$ for NBD and GMD are given in Refs. 4 and 5, respectively.

(ii) For pure gluon bremsstrahlung, we have $\bar{n}(k)=k'e^{At}$ where $A=B=C=k=0$, the general solution, Eq. (8) reduces to the Furry-Yule distribution (FYD) (Refs. 3 and 6)

$$P_n(\bar{n},k',0)=\frac{\Gamma(n)}{\Gamma(n-k'+1)\Gamma(k')}\times\left[\frac{\bar{n}-k'}{\bar{n}}\right]^{n-k'}\left[\frac{k'}{\bar{n}}\right]^{k'}, \tag{11}$$

where $k'\leq n$. Hwa and Lam[7] suggest using this distribution to fit multiplicity distribution of pp and $p\bar{p}$ collisions. Below we give the $C_q(q=2-5)$ normalized moments:

$$C_2=\frac{1-2k'/\bar{n}+k'}{k'}+\frac{1}{\bar{n}}, \tag{12}$$

$$C_3=\frac{6(1-k'/\bar{n})^2}{k'^2}+\frac{6(k'-1)(1-k'/\bar{n})}{k'^2}+\frac{(k'-1)(k'-2)}{k'^2}+\frac{6(1-k'/\bar{n})}{k'}\left[\frac{1}{\bar{n}}\right]+\frac{3(k'-1)}{k'}\left[\frac{1}{\bar{n}}\right]+\frac{1}{\bar{n}^2}, \tag{13}$$

TABLE IV. C_q moments computed from GMD, NBD, and FYD at 200 GeV (limited pseudorapidity range).

	GMD				NBD				FYD			
η_c	C_2	C_3	C_4	C_5	C_2	C_3	C_4	C_5	C_2	C_3	C_4	C_5
0.5	1.80	4.40	12.87	42.54	1.81	4.40	12.87	42.50	1.73	4.02	11.59	38.27
1.5	1.53	3.10	7.56	21.11	1.54	3.10	7.58	21.17	1.63	3.80	10.71	33.97
3.0	1.32	2.18	4.20	9.01	1.32	2.19	4.21	9.00	1.26	2.44	5.43	13.19
5.0	1.21	1.79	3.00	5.52	1.22	1.80	3.02	5.55	1.02	1.73	3.31	6.84

TABLE V. C_q moments computed from GMD, NBD, and FYD at 546 GeV (limited pseudorapidity range).

	GMD				NBD				FYD			
η_c	C_2	C_3	C_4	C_5	C_2	C_3	C_4	C_5	C_2	C_3	C_4	C_5
0.5	1.88	4.86	15.82	60.84	1.89	4.96	16.65	67.88	1.65	4.00	12.65	48.14
1.5	1.55	3.21	8.14	24.13	1.62	3.57	9.90	33.12	1.89	5.35	20.08	93.01
3.0	1.44	2.69	6.08	15.84	1.46	2.76	6.43	17.66	1.65	3.92	11.20	35.76
5.0	1.34	2.24	4.40	9.79	1.36	2.31	4.69	10.99	1.44	3.04	7.54	20.55

$$C_4=\frac{24(1-k'/\bar{n})^3}{k'^3}+\frac{36(k'-1)(1-k'/\bar{n})^2}{k'^3}+\frac{12(k'-1)(k'-2)(1-k'/\bar{n})}{k'^3}$$
$$+\frac{(k'-1)(k'-2)(k'-3)}{k'^3}+\frac{36(1-k'/\bar{n})^2}{k'^2}\left[\frac{1}{\bar{n}}\right]+\frac{36(k'-1)(1-k'/\bar{n})}{k'^2}\left[\frac{1}{\bar{n}}\right]$$
$$+\frac{6(k'-1)(k'-2)}{k'^2}\left[\frac{1}{\bar{n}}\right]+\frac{14(1-k'/\bar{n})}{k'}\frac{1}{\bar{n}^2}+\frac{7(k'-1)}{k'}\left[\frac{1}{\bar{n}^2}\right]+\frac{1}{\bar{n}^3}\,, \tag{14}$$

$$C_5=\frac{120(1-k'/\bar{n})^4}{k'^4}+\frac{240(k'-1)(1-k'/\bar{n})^3}{k'^4}+\frac{120(k'-1)(k-2)(1-k'/\bar{n})^2}{k'^4}$$
$$+\frac{20(k'-1)(k'-2)(k'-3)(1-k'/\bar{n})}{k'^4}+\frac{(k'-1)(k'-2)(k'-3)(k'-4)}{k'^4}$$
$$+\frac{240(1-k'/\bar{n})^3}{k'^3}\left[\frac{1}{\bar{n}}\right]+\frac{360(k'-1)(1-k'/\bar{n})^2}{k'^3}\left[\frac{1}{\bar{n}}\right]+\frac{120(k'-1)(k'-2)(1-k'/\bar{n})}{k'^3}\left[\frac{1}{\bar{n}}\right]$$
$$+\frac{10(k'-1)(k'-2)(k'-3)}{k'^3}\left[\frac{1}{\bar{n}}\right]+\frac{150(1-k'/\bar{n})^2}{k'^2}\left[\frac{1}{\bar{n}^2}\right]+\frac{150(k'-1)(1-k'/\bar{n})}{k'^2}\left[\frac{1}{\bar{n}^2}\right]$$
$$+\frac{25(k'-1)(k'-2)}{k'^2}\left[\frac{1}{\bar{n}^2}\right]+\frac{30(1-k'/\bar{n})}{k'}\left[\frac{1}{\bar{n}^3}\right]+\frac{15(k'-1)}{k'}\left[\frac{1}{\bar{n}^3}\right]+\frac{1}{\bar{n}^4}\,. \tag{15}$$

III. RESULTS AND COMMENTS

In this paper besides the GMD analysis, we also examine the FYD and comparisons are made with NBD and experimental (NSD) data. The distributions are all described by Koba-Nielson-Olesen (KNO) scaling variables: namely, the product of the mean charged multiplicity $\bar{n}$ and the probability of n charged particles as functions of the scaled variable $z=n/\bar{n}$. However, UA5 has reported KNO-scaling violation at 200, 546, and 900 GeV (Refs. 1 and 8).

Whenever possible, efforts were made to obtain the best χ^2/points fits by allowing both k' and k to vary. Minimum χ^2/points and the comparison of moments C_q with that obtained from experiment will indicate the best fits. χ^2/points for the limited pseudorapidity intervals, η_c at 200, 546, and 900 GeV are given in Tables I–III and Figs. 1–12.

For all energies and intervals, the χ^2/points for NBD and GMD are equally good whereas for FYD, not all the fits are acceptable (note again, that FYD and NBD are special cases of GMD).

We want to point out that both GMD [Eq. (8)] and FYD [Eq. (11)] are restrained by $n \geq k'$ due to the nature of both equations. Hence, to admit a k' value of unity we have to neglect the first point, $n=0$ in our computation. Observing this behavior of k' for FYD, k' seems to "push" beyond unity for a comparable χ^2/point fit. Indeed the fits improve tremendously for FYD as shown in Tables I–III when a further second point, $n=1$, is

TABLE VI. C_q moments computed from GMD, NBD, and FYD at 900 GeV (limited pseudorapidity range).

	GMD				NBD				FYD			
η_c	C_2	C_3	C_4	C_5	C_2	C_3	C_4	C_5	C_2	C_3	C_4	C_5
0.5	1.84	4.70	14.70	52.88	1.85	4.72	14.77	53.02	1.66	3.96	11.96	42.01
1.5	1.58	3.34	8.58	25.08	1.58	3.36	8.62	25.24	1.64	3.88	11.01	35.10
3.0	1.35	2.38	4.91	11.23	1.36	2.41	4.96	11.36	1.29	2.53	5.75	14.22
5.0	1.25	1.96	3.53	7.01	1.25	1.96	3.52	6.96	1.10	1.95	3.94	8.60

TABLE VII. Comparison of χ^2/points for GMD, NBD, and FYD at 200, 546, and 900 GeV (full phase space) and within parentheses the numbers of data points being taken.

Full space		GMD			NBD		FYD	
$\sqrt{s}$	$\langle n \rangle$	k'	k	χ^2/points	k	χ^2/points	k'	χ^2/points
200 GeV	21.40	1.50	2.43	0.26 (28)	4.56	0.30 (28)	2.00	5.65 (28)
							3.28	0.24 (27)
546 GeV	29.40	2.00	1.44	1.05 (41)	4.06	1.31 (41)	2.00	24.99 (41)
							3.13	0.94 (40)
900 GeV	35.60	2.00	1.19	1.33 (50)	3.55	1.53 (50)	2.00	6.03 (50)
		2.50	0.60	1.29 (49)			3.02	1.24 (49)

neglected in all the intervals.

However, in the minimum χ^2/points computation for GMD, only $n=0$ is neglected because the restriction on initial number of gluons k' by the hadron multiplicity n can be compensated by k, which is related to the initial number of m quarks.

In all the pseudorapidity ranges k (NBD) and k' (FYD) increase with η_c as shown in Tables I–III. Also both k and k' deviate from integer values with the exception of FYD due to the above comments. For GMD we do not expect k and k' to be integers if interpreted in the average sense.[2] The trends of k' and k in GMD in relation to η_c are still hard to see (although we would expect k' to increase with η_c). Whereas k (NBD) increases rather linearly with η_c in all the energies as shown in Figs. 19–21. For FYD, k' increases as η_c grows but flattens at 2.00 (if $n=1$ is removed) as shown in Tables I–III.

At 546 GeV in Table II, the k' in FYD is able to rise above 2.0 because data points n were given in steps of 3 ($n=1,4,7,\ldots$). Hence neglecting the first point, n starts with 4 and gives k' a greater flexibility to vary. The experimental (NSD) data at this energy are given in Refs. 9 and 10. A more detailed analysis of GMD at 540 GeV pseudorapidity ranges can be found in Ref. 5. UA5 (Ref. 9) reported that the NBD fits extremely well which is also supported by the fact that k' is very small when GMD is employed to get the best χ^2/points fit.[5]

FYD fits are never good for small pseudorapidity ranges even if two first points are neglected in all three energies as shown in Tables I–III. The χ^2/points fits improve for all the energies as intervals enlarge as shown in comparing Tables I–III and Table VII.

C_q, normalized moments are tabulated in Tables IV–VI and comparisons were made with the experimental data in Figs. 16–18. In all energies, the moments increase as the η_c decreases and becomes more pronounced for the smaller pseudorapidity intervals.

Figure 24 gives the C_q (GMD) moments at various energies. C_q moments increase with energy (KNO violation) as shown in Tables VIII and IX.

Clearly one could see that both k (NBD) and k' (FYD) decrease with increase in energy $\sqrt{s}$ as shown in Table VII and Fig. 22. Table IX gives possible values of k' and k (GMD) which gives reasonable fits for pp collisions at ISR energies.[11] χ^2/points given for 52 and 62 GeV are best fits. k', occurs ~ 0.50. k' (GMD) and k (GMD) are inversely related to each other with k (GMD) approaching zero while k' (GMD) approaches 3.00 as $\sqrt{s}$ moves to the TeV region as shown in Figs. 23 and 24. However k' (FYD) and k (NBD) also tend to a limit of ~ 3.00 as shown in Fig. 22 (minus $n=0,2$).

Figures 13–15 give the three distributions for full space, computed for the same number of data points. Note that in all three energies FYD peaks are shifted to the left and lower than the other two distributions. For 200 and 546 GeV, the peak for GMD and FYD occur at the same position as the data while at 900 GeV the experimental peak is shifted slightly away from them.

Figure 15 gives a significant experimental peak which all the three distributions fail to reach. The highest is given by GMD.

IV. DISCUSSION AND CONCLUSION

In GMD we identify k to be related to m initial number of quarks by $k=m\tilde{A}/A$ [Eq. (6)], noting that it is possible for $k \geq m$ or $k \leq m$ depending on whether quark branching ($q \rightarrow q+g$) or gluon branching ($g \rightarrow g+g$) dominate, respectively. Interpreting k this way will do away with the fact that k needs to be an integer in the case of interpreting k as independent phase-space cells.

The fact that NBD fits experimental data well at 200 and 546 GeV at all pseudorapidity intervals implies quarks branching dominate. This is consistent because the FYD which gives the other extreme of $k=0$, suggest-

TABLE VIII. C_q moments computed from GMD, NBD, and FYD at 200, 546, and 900 GeV (full phase space).

	GMD				NBD				FYD			
$\sqrt{s}$	C_2	C_3	C_4	C_5	C_2	C_3	C_4	C_5	C_2	C_3	C_4	C_5
200 GeV	1.20	1.72	2.80	4.99	1.20	1.74	2.82	5.03	1.17	1.82	3.23	6.24
546 GeV	1.22	1.81	3.06	5.72	1.23	1.81	3.05	5.66	1.22	1.97	3.64	7.36
900 GeV	1.23	1.85	3.18	6.05	1.24	1.87	3.22	6.11	1.22	1.98	3.68	7.49

TABLE IX. Computation for GMD at CERN ISR energies (pp) and within parentheses the numbers of data points being taken.

	Generalized multiplicity distribution (GMD)				(pp ISR energies)			
$\sqrt{s}$	$\langle n \rangle$	k'	k	χ^2/points	C_2	C_3	C_4	C_5
30.4	10.54	0.50	9.11	1.28 (17)	1.18	1.60	2.44	4.09
44.5	12.08	0.50	7.66	0.48 (19)	1.19	1.63	2.51	4.28
52.6	12.76	0.50	6.58	0.26 (21)	1.20	1.68	2.66	4.68
62.6	13.63	0.50	7.10	1.46 (20)	1.19	1.62	2.50	4.24

ing gluon branching is not likely to dominate due to large χ^2 fits. This is also true for small intervals of 900 GeV. However, as η_c increases we do observe increase in initial number of gluons (k') as shown in Tables I and II which gives equally good fits for GMD.

It is useful to note that FYD does not have the great flexibility of the NBD and GMD. First k' is controlled by n, the hadron multiplicity. Second, notice that with the introduction of initial number of gluon in GMD for all intervals, the χ^2 fits do not seem to change very much as shown in Tables I–III.

The above behavior of quarks (k) and gluons (k') also applies to 900 GeV in Table III, except that for $\eta_c = 3.0, 5.0$ and full phase space, there is an unexplained high peak.

Interpreting $k = m\tilde{A}/A$ could explain why the parameter k decreases with energy. There have been reports that energies increase with the gluon contribution to the minijet cross section.[12] Hence gluon branching A would be dominant over quark $\tilde{A}$ branching. Figure 23 shows as initial number of gluons k' (GMD) increases, k (GMD) decreases which is consistent with the experiment. It is predicted that as energy moves into TeV region, k (GMD) approaches zero as shown in Fig. 23 while the gluons k' (GMD) tends to a maximum limit of above 3.0. Thus making gluon branching a dominant feature in TeV colliders. This implies that Furry-Yule distribution will provide a good description for higher TeV region.

From the above argument, the widening of the generalized multiplicity distribution (GMD) will stop in TeV region as k is expected to be constant. It is clear that Eq. (5), which GMD satisfies, comprises two processes, namely, when $\tilde{A} = 0$ we have a Furry-Yule process

$$\left[\frac{\partial P_{m,n}(t)}{\partial t} = A(n-1)P_{m,n-1}(t) - AnP_{m,n}(t) \right]$$

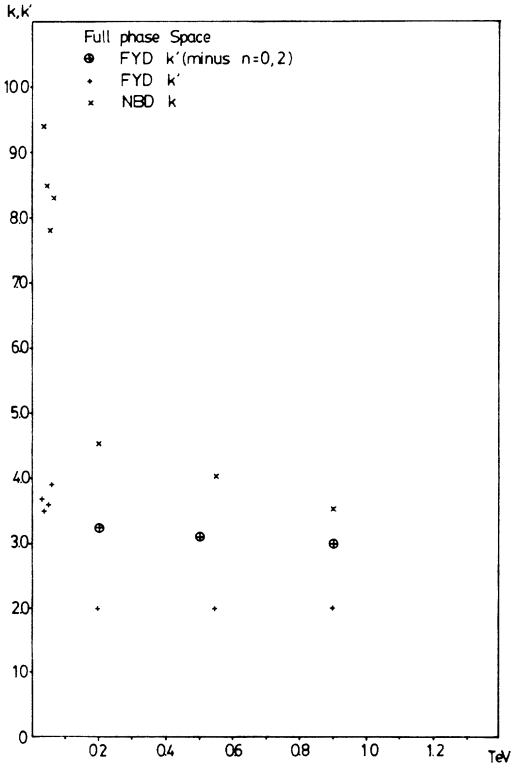

FIG. 22. k (NBD) and k' (FYD) plotted against $\sqrt{s}$ energies.

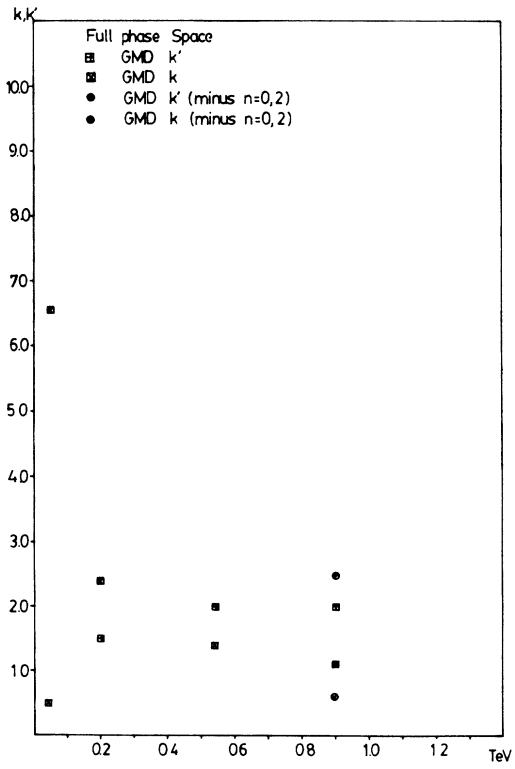

FIG. 23. k (GMD) and k' (GMD) plotted against $\sqrt{s}$ energies.

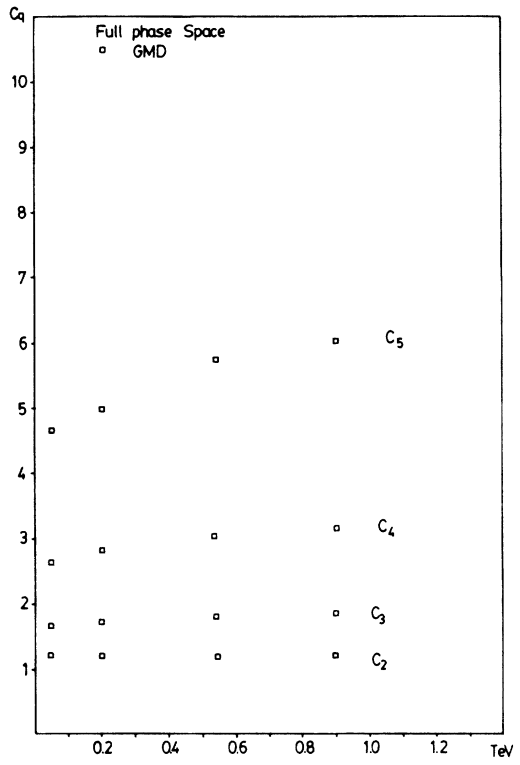

FIG. 24. C_q moments as a function of $\sqrt{s}$ energies.

where $A=0$ gives the Poisson process

$$\left[\frac{\partial P_{m,n}(t)}{\partial t}=\tilde{A}\tilde{m}P_{m,n-1}(t)-\tilde{A}\tilde{m}P_{m,n}(t)\right].$$

In the perspective of the above comment, k decreases with energy would imply $A>\tilde{A}$ and further implies the dominance of the Furry-Yule process over the Poisson process. However, for limited pseudorapidity ranges at each energy this is not so, k increases with η_c (Figs. 19–21, Tables I–III) and k' dependence on η_c is still hard to ascertain especially for 546 GeV. But we expect k' to increase slowly with η_c as indicated in Tables I and III for 200 and 900 GeV. The range of k' is always $0\le k'\le n$. This means that the Poisson process becomes the primary process as ranges widen. Similar branching model has been studied[13] and the dynamical origin of the energy dependence of the initial number of quarks and gluons has also been addressed. A note here will be k' is the initial number of gluons but k is only related to m the initial number of quarks.

In summary, the negative-binomial distribution provides excellent fits to limited pseudorapidity range and the full phase space at 300 and 546 GeV, and also for 900 GeV at small η_c intervals. For large η_c intervals and full phase space at 900 GeV, the generalized multiplicity distribution provides a slightly better fit than the NBD and the high peak in experimental data is suspected to be due to the inclusion of minijets in the treatment of data. As collider energies usher in the TeV era, the GMD will approach the Furry-Yule distribution because the gluon contribution will be significant.

The generalized multiplicity distribution may provide an alternative distribution to the NBD for future NSD data obtained from TeV colliders. This distribution can also offer an explanation for e^+e^- data in which NBD fits so well, as in the initial stages of the annihilation, where quark k dominates while gluon k' contribution is zero.[2,4]

[1]UA5 Collaboration, R. E. Ansorge *et al.*, Z. Phys. C **43**, 357 (1989).
[2]C. K. Chew, D. Kiang, and H. Zhou, Phys. Lett. B **186**, 411 (1987).
[3]B. Durand and I. Sarcevic, Phys. Lett. B **172**, 104 (1986).
[4]C. K. Chew and Y. K. Lim, Phys. Lett. **163B**, 257 (1985).
[5]A. H. Chan and C. K. Chew, Nuovo Cimento **101A**, 409 (1989).
[6]A. Giovannini, Nucl. Phys. **B161**, 429 (1979).
[7]R. C. Hwa and C. S. Lam. Phys. Lett. B **173**, 346 (1986).
[8]UA5 Collaboration, G. J. Alner *et al.*, Phys. Rep. **154**, 247 (1987).
[9]UA5 Collaboration, G. J. Alner *et al.*, Phys. Lett. **160B**, 193 (1985); **160B**, 199 (1985).
[10]B. Asman, Ph.D. thesis, University of Stockholm, Report No. 85-17.
[11]ISR Collaboration, A. Breakstone *et al.*, Phys. Rev. D **30**, 528 (1984).
[12]UA1 Collaboration, C. Albajar *et al.*, Nucl. Phys. **B309**, 405 (1989).
[13]I. Sarcevic, Phys. Rev. Lett. **59**, 403 (1987).